The prospects for additive manufacturing of bulk TiAl alloy

M. Thomas, T. Malot, P. Aubry, C. Colin, T. Vilaro, Pierre Bertrand

The Prospects for Additively Manufacturing Bulk TiAl Alloy

M. Thomas[1*], T. Malot[2], P. Aubry[3], C. Colin[4], T. Vilaro[5]
P. Bertrand[6]
[1]ONERA, Chatillon, France
[2]ENSAM, Paris, France
[3]CEA/DEN/DANS/DPC/SEARS/LISL, Saclay, France
[4]Mines ParisTech, Paris, France
[5]Airbus, Toulouse, France
[6]ENISE, St Etienne, France

* corresponding author : email marc.thomas@onera.fr

Keywords: gamma titanium aluminide, selective laser melting, laser metal deposition, electron beam melting, heat treatments

This paper deals with the prospects for additive manufacturing (AM) of bulk TiAl alloys. A number of AM processes have already been explored in the literature for these intermetallic alloys. The main trend developed in published works concerns a strong crack sensitivity of this relatively brittle material due to rapid successive heating and cooling cycles. Optimized processing conditions have already been achieved for producing sound and crack-free TiAl materials by means of EBM and LMD processes. This experimental work was particularly focused on the third process, *i.e.* SLM, to produce fully dense TiAl parts. A series of beads, surface layers and cubes have been manufactured to investigate the microstructural evolution. Post heat treatments allowed a uniform microstructure to be restored for the intermetallic TiAl alloy.

1. Introduction

Regarding the development of advanced materials, the manufacturing techniques cover the compositional and microstructural aspects to satisfy the industrial requirements, but also the shape building aspect to achieve the geometrical, technical and functional properties of components. Thus, attempts are currently made in the aerospace sector to meet such property requirements by using near net or net shape processing.

Due to the rapid progress made in the field of Additive Manufacturing (AM) these last years, such technologies seem suitable to manufacture net shape and fully dense complex metallic components.

The attractiveness of these direct manufacturing technologies is that it reduces the time to market of products with no specific tooling required. Practically, most of the AM processes start from a precursor powder that is consolidated layer-by-layer using directly a three dimensional computer aided design (CAD) data file. In the case of aeroengine components, AM is highly appealing for several reasons. First of all, it allows a better buy-to-fly ratio owing to a low material waste factor. Secondly, AM shortens the lead time by reducing machining and joining steps and by avoiding time consuming tooling reworking. Thirdly, it allows weight saving and additional functionalities by adding supplementary fonctions such as cooling channels. Hence, AM already appears as a cost-effective processing route for a number of existing aeroengine components.

Available techniques for metals are laser metal deposition (LMD), electron beam melting (EBM), and selective laser melting (SLM). For laser metal deposition (LMD) process, the powder is injected through a nozzle onto the substrate to be molten layer by layer. The other two processes (SLM and EBM) consist of creating a powder bed where the powder is deposited through a roller or a blade into a compacted layer which is then selectively melted by the scanned laser or electron beam, with the part being built up layer by layer.

Now, for an improved energy efficiency and power in gas turbine engines, an increase of their maximum work temperature is required. Therefore, the development of advanced materials with high temperature resistance such as gamma titanium aluminides attracted considerable attention in the last two decades. Due to their ordered structure and to their lightweight, this family of intermetallic alloys exhibits a good combination of properties, such as a high melting point, low density and strength at temperatures up to ~750°C [1]. Recently, the Ti-(47-48)Al-2Cr-2Nb alloy has been introduced in the low pressure (LP) turbine of the GEnX jet engine (General Electric) which powers Boeing787 and 747-8 [2].

It is recalled that the conventional processing route for LP turbine blades is either gravity or centrifugal casting. The latter is preferred to limit the formation of gas porosities and of mis-runs. However, cast processing generally yields a relatively coarse microstructure with metallurgical defects such as porosity shrinkage. This leads to relatively poor room-temperature mechanical properties, in particular low ductility and toughness. The lack of ductility also renders machining difficult. Moreover, wide property variability is generally observed for different thickness of cast parts and location of test specimens. In a general manner, these casting related features might restrict the use of γ-TiAl alloys to simple shape and moderate dimension. Therefore, alternative

processing routes, including AM technologies, have been investigated with the aim to produce complex shaped TiAl components with a more uniform microstructure. A number of experimental studies already deal with the process of γ-TiAl by means of Additive Manufacturing (AM).

1° LMD or cladding process

In the mid-nineties, methods for joining and for surface modification were investigated by laser welding for a Ti-46Al-2Mo alloy [3]. Crack-free welds could be obtained only for low scan rates and with pre-heating temperatures above 400°C. First laser cladding trials that have been carried out on titanium aluminide alloys range back to the late nineties [4]. In a general manner, laser cladding operations were aimed at overlaying a base material, typically TA6V, with TiAl to form a protective layer against oxidation. Dilution rate is an important factor since some dilution is required to guarantee a sound metallurgical bond, but in a limited extent to reduce the problems associated with distortion and a brittle heat-affected zone. For instance, in a more recent work of laser cladding coatings of Ti-48Al-2Cr-2Nb alloy on Ti6Al4V, some dilution with base material that may degrade coating properties, was observed since the coating composition (Ti-46Al-2Cr-2Nb at.%.) was slightly richer in Ti than the original powder (Ti-48Al-2Cr-2Nb at.%.) [5]. However, most of their work was based on the important cracking sensitivity of this intermetallic material. By using penetrating fluid tests for single tracks, uncracked conditions were identified by using lower powder feed rate and lower scanning speed. This was related to the decreased cooling rate for lower scanning speed which prevents cracking. In addition, the authors reported that heating previously and during the process tends to improve the results in terms of cracking.

The LMD process was also evaluated to process bulk Ti-47Al-2Cr-2Nb samples [6]. Provided a continuous deposition was ensured, thermal stresses were reduced and the deposited material contained no cracks. However, not much detail is given about the process parameters. Subsequent heat treatments with super-transus conditions, i.e. in the single α phase field, were then performed to homogenize the microstructure. However, this did not seem to improve tensile properties with respect to the as-built condition. In the meantime, Srivastava et al have demonstrated that the heterogeneous microstructure of a laser fabricated Ti-48Al-2Mn-2Nb alloy was associated with the many thermal excursions as the successive layers are deposited [7]. For this particular alloy, the processing parameters that have significant effects on the quality of the component have been identified [8]. The amount of laser energy and the volume of powder were found to determine the stability of the build-up rate and therefore the uniformity of build geometry and quality [9]. However, crack-free samples and a good quality surface finish were not achieved in their work.

According to Zhang *et al*, the focus of the powders must be below the deposition plane for an optimum performance in terms of build-up rate and coupling of the deposit to the substrate [10]. It was also found in this study for the Ti-48Al-2Cr-2Nb alloy that each deposited layer consists of a metastable microstructure with the massive γ phase on the top of the layer while the high temperature α-phase, which is then ordered to α_2-Ti_3Al, was retained on the bottom of the layer. Much higher cooling rate was obtained at the bottom of the layer because of a rapid rate of heat extraction.

The directionality of thermal gradients along the Z-built axis tends to favour texture effects. For the stoichiometric binary TiAl alloy, sequential laser remelting tends to create the directional growth of metastable γ phase with (111) plane perpendicular to the thermal gradient direction [11]. Qu *et al* investigated the phase transformation for the Ti–47Al–2.5V–1Cr alloy manufactured by LMD [12]. A directionally solidified columnar grain structure was formed in the deposition direction due to the high temperature gradient. Subsequent solid state phase transformation took place in the heat affected zone of the deposited material and led to the formation of a fully lamellar microstructure with colony size in the range of 50–100 μm and lamellar spacing of 0.3–0.5 μm. At room temperature, a lack of tensile ductility (0.6%) was observed in both longitudinal and transverse sections of the as-deposited samples. The authors further investigated the effect of heat treatments using the same Ti–47Al–2.5V–1Cr alloy [13]. However, the compositional inhomogeneity of the as-deposited samples were not completely removed after heat treating at 1125°C for 30 min. So, the tensile ductility of test samples was not really improved by this heat treatment at low temperature, with maximum values of 0.6%.

2° The EBM process

Regarding now the development of the EBM process, first attempts to consolidate Ti-47Al-2Cr-2Nb powder were made by Cormier [14-15]. This earlier work revealed a dramatic decrease of aluminium from 46 at.% to 39 at.% by comparing the original powder with the EBM-fabricated test sample. This is related to the fact that aluminium is a volatile element with high vapor pressure, which is evaporated from the surface due to the vacuum exposure. However, it is difficult to identify a clear trend in their work about the Al loss conditions because of the scarce information given on the process.

Murr *et al* have characterized Ti–47Al–2Cr–2Nb coupons that were produced by electron beam melting (EBM) [16]. Residual porosity was attributed both to non-optimized build conditions and to Ar bubbles from the atomised powder. Surprisingly, the authors did not observe any changes in the chemistry of the coupons compared to the original powder, in particular no aluminium loss. This is presumably due to the fact that the EBM machine did operate without multiple melt passes required for optimized settings.

Rastkar *et al* evaluated the possibility of making hard surface layers by using EBM with a Ti–45Al–2Nb–2Mn–1B alloy [17]. By using high power and high scanning speed, the cooling rate is fast enough to largely suppress α to α_2 phase transformation and promote a microstructure with the hard ordered B2 phase. On the other hand, a decreased scanning speed induces higher local superheat, thereby increasing the evaporation of aluminium [18]. Ge *et al* also reported the strong influence of energy input on Al evaporation for Ti-47Al-2Cr-2Nb powders [19]. An Al loss up to 15 at.% was observed at the highest energy input. As a consequence, the phase transformation in samples was really different depending on the energy input.

Biamano *et al* investigated the possibility to produce fully dense near-net-shape parts made of the Ti-48Al-2Cr-2Nb alloy composition [20]. A process optimization was needed to completely eliminate the residual porosity located between two subsequent layers. However, smaller spherical pores were found to remain in the powder particles due to argon gas entrapment during the atomization process. In parallel, the Al loss was reported to be approximately 1 at.%. The as-built samples were then hot isostatically pressed (HIPed) at 1260°C under a pressure of 170 MPa for 4 h, thus reducing the residual porosity down to 1%. A beneficial effect of HIP and subsequent heat treatment at 1320°C for 2 hours was to significantly reduce the data scattering in tensile properties, i.e. down to 6% for YS at room temperature.

Schwerdtfeger *et al* made a comprehensive study of the effect of EBM process parameters on the resulting microstructures and on the Al loss of the Ti-48Al-2Cr-2Nb alloy [21]. A too high energy input should not be recommended, first because this results in insufficient interlayer connection due to significant differences in powder layer thickness deposited in the successive layers, and second because of a higher Al evaporation. Attempts were then made to decrease overheating in the melt pool for an expected reduced Al evaporation. Under optimized processing conditions, an Al loss as low as 0.5 at.% was then achieved. In more details, a decrease in overheating was obtained by lowering layer thickness and by increasing scan speed. However, this limited Al loss is obtained at the expense of the microstructure because the preferred lamellar microstructure with small colony

sizes tends to develop for low scan speeds. Furthermore, because the Al evaporation takes place in the top region of the melt pool, an inhomogeneous distribution of Al element cannot be prevented through the sample height. Local variations in the Al concentration can then affect the solidification pathway and subsequently the size and morphology of the microstructure.

A high niobium content alloy was also investigated for blade production and mechanical testing [22]. In the as-built condition, the Ti-45Al-8Nb-2Cr alloy develops a fully lamellar microstructure with lamellar grains of about 100 μm. A higher oxidation resistance was also reported for this alloy with respect to Ti-48Al-2Cr-2Nb. Test results on blades show that FE prediction of critical location is correct and fatigue limit is comparable with the values obtained on test samples.

3° The SLM process

Whereas the SLM process is already used for a number of metallic materials (steels, titanium alloys, nickel base superalloys, cobalt chromium and aluminum alloys), it has not been demonstrated so far as a suitable process for γ-TiAl alloys. In 2011, Löber *et al* made some attempts of SLM processing of a Ti-48Al-2Cr-2Nb alloy which resulted in multi-cracks samples [23]. More recently, Löber *et al* used a TNM alloy composition which is also susceptible to cracking because of the small volume fraction of β-phase as the starting powder [24]. A very limited fraction size of powder (45–63 μm) with a layer thickness of 75 μm was used. Laser power and scanning speed were adapted to stabilize the process and to obtain the best morphology for single beads. Fragmentation of the beads, the so-called balling effect, was reported at low laser power (50 W) and low scanning speeds (50–100 mm/s), but also at intermediate laser power (100 W) and very high scanning speeds (350–2100 mm/s). Pronounced cracking which was related to high cooling rate during solidification, was also observed at low power and low scanning speeds (150–300 mm/s). A set of process parameters in an intermediate range (scanning speed: 150–300 mm/s; laser power: 100–250 W) was identified to generate stable beads without fragmentation or crack formation. Now, because of a non-uniform cooling rate during the SLM process, the microstructure was found to be inhomogeneous with coarser and finer regions next to each other. A two-step heat treatment caused a microstructural homogenization in the first step at 1230°C in the α/β-region and allowed the precipitation of γ lamellae in the second step at 950°C. Subsequent to this heat treatment, a duplex microstructure consisting of β and α_2 grains with some γ lamellae in α_2/γ colonies is obtained.

In these prior investigations, one can note that no much work was devoted to AM of bulk TiAl materials. In a recent paper, it has been demonstrated that optimal process parameters can be

determined for LMD process to prevent cracking due to built-up residual stresses during fast cooling [25]. Post heat-treatments were then used to restore homogeneous lamellar or duplex microstructures. Subsequent room temperature tensile tests provided a good validation of the TiAl material soundness and homogeneity. Based on this promising result with the LMD process, the present work is aimed at investigating the influence of the SLM process parameters for the commercial Ti-47Al-2Cr-2Nb (at.%) alloy in order to produce fully dense parts without cracking. Conventional post-heat treatments were also given to the as-built material in order to homogenize the microstructure.

2. Experimental procedure

The atomised powder was sieved to collect powder particles smaller than 50 μm. Chemical analysis of the selected powder which was performed by plasma emission (ICP) is given in Table I. The SLM tests were carried out by means of a Phenix PM100 machine. Successive powder layers of 60 μm high were deposited without any additional densification of the layer. To prevent any melt pool oxidation, a neutral atmosphere was maintained in the process chamber with an argon flow of 50 l / min. A series of experiments have been performed to identify the effect of process parameters such as the scan speed, the diameter of the laser beam, the overlapping ratio and the preheating temperature of the TA6V substrate. Our purpose was to identify the range of values of individual processing parameters for which stable build-up rate can be obtained.

Table I : Chemical analyses of the initial powder

Ti (at%)	Al (at%)	Cr (at%)	Nb (at%)	Fe (at%)	C / ppm	O / ppm
48.5	47.21	2.12	2.11	0.03	105	745

For microstructural observations, samples were cut by electro discharge machining, then embedded in a conductive resin for subsequent mechanical polishing until a mirror finished-surface was obtained. SEM observations of un-etched specimens were performed on a Zeiss 962 DSM equipment, by using either back-scattered or secondary electron conditions. For optical observations, some samples were etched with the Kroll reagent to reveal the microstructure as well as the metallurgical defects.

Experiments were also conducted on the possibility of recycling the powder by using the unmelted powder during the built. The oxygen content and the morphology of recycled powder particles were analyzed. For this investigation, conductive pads were used to seize the powder on the substrate after each laser melt.

3. Experimental results

The first process parameter to be considered was the speed of the laser beam, which can affect the morphology of the molten bead. Different scanning speeds ranging from 10 mm/s to 160mm/s have been compared in Figure 1. Irregular beads are produced with low speeds as illustrated in Figure 1a. An increasing scanning speed tends to reduce the apparent width of the bead. At intermediate speeds, the bead formation remains stable as revealed in Figure 1b. Scanning speeds between 30 and 60 mm/s yield the most stable bead. On the other hand, higher scanning speeds induce a fragmentation effect which is characterized by elongated molten discontinuous materials as shown in Figure 1d. This instability of melt pool is probably due to surface tension, which favors the formation of a fragmented bead. It is interesting to note that these different beads showed no visible crack using optical microscopy.

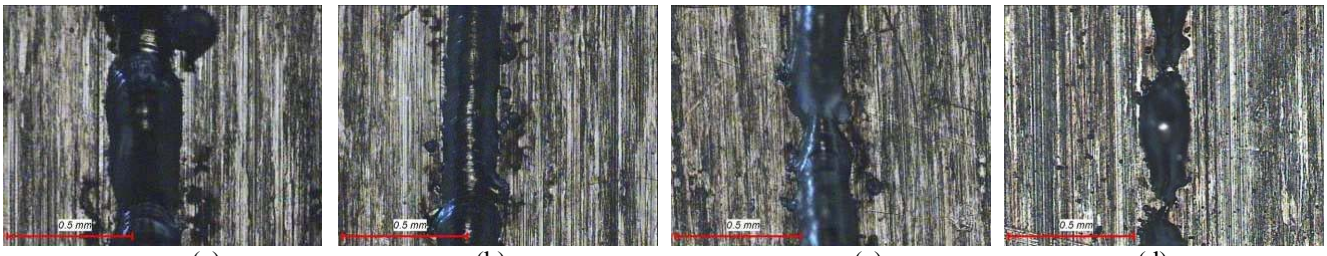

(a) (b) (c) (d)

Figure 1: Optical microscopy of beads manufactured by SLM with different speeds: (a): 10 mm / s; (b): 50 mm / s; (c): 70 mm / s; (d): 160 mm / s

In a second stage, XY 10 * 10 mm surface layers have been produced with different overlapping ratios according to the favorable scanning speeds. The overlapping ratio cannot be optimized independently of the scanning speed since a lower speed results in wider beads. The optimised overlapping ratio was determined by comparing different overlapping ratios from 0 to 30% between adjacent beads. A too high overlapping ratio contributes to significantly increase the lead time. Conversely, if the overlapping is not sufficient, then this can lead to the formation of elongated cavities in the solid sample, as observed in Figure 2. The last stage which corresponds to the manufacturing of bulk cubic samples, was conducted for an overlapping ratio of 25%.

Figure 2: Optical microscopy of XY surface layers using the following parameters: power 50 W, speed 60 mm/s, distance between two laser lines 200 µm

To overcome the problem of porosities for low overlapping ratio, a "double melting" strategy was investigated. This consists of a second laser scanning over the entire surface before adding the next powder layer in order to smooth the surface. Indeed, melting the surface by laser is a method applied industrially for improving the roughness. However, this built strategy was found to enhance the risk of interrupted laser due to the high reflectivity of smooth surfaces. Consequently, a "cross strategy" was adopted, even though the surface roughness was not so good as illustrated in Figure 3. Moreover, the process chamber was pre-heated at 200°C to allow the residual stresses to be relieved during the process due to the cracking sensitivity of the TiAl material.

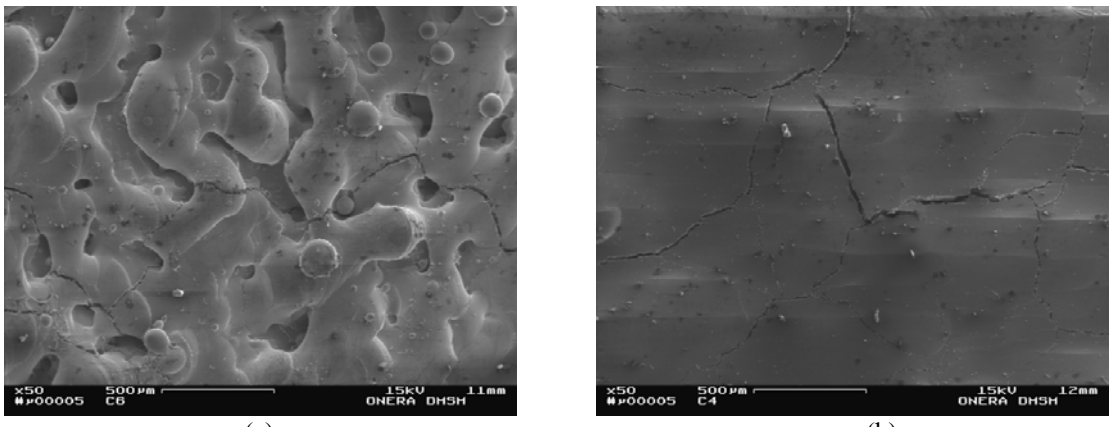

(a) (b)

Figure 3 : SEM micrographs using secondary electrons of the surface of SLM samples using the following parameters: power 50 W, speed 50 mm/s, distance between beads 160 µm: (a) : cross-strategy ;(b) : double melting strategy

With these optimized parameters, a number of 10*10*10 mm cubes have been produced with a height of 10 mm. After examination of potential defects, a network of regular cracks have been

detected in the series of cubes. A visual measurement of the average distance between cracks was taken as a criteria in order to identify the best processing conditions. It appears that the distance between cracks is reduced, i.e. the number of cracks is increased for higher speeds. This is consistent with the fact that the residual stresses are higher at high speeds, which logically generate more cracks. On the other hand, the average distance between the cracks does not clearly change for different overlapping ratios.

Even if the speed of the laser beam is the predominant parameter for the total energy absorbed by the material, the microstructural evolutions for different scanning speeds are relatively low. Quite expectedly, a higher speed produces a slightly finer microstructure.

As emphasized previously in some published works, the intermetallic TiAl alloy tends to crack during multiple heating and cooling cycles due to fast cooling rate. Therefore, processing conditions that induces a lower temperature gradient of the solidification front should be favorable to prevent cracking. Thus, an extended time of interaction between the laser beam and the powder should decrease the cooling rate. However, the cooling rate is higher by SLM than by LMD. For instance, by SLM it seems that a delay time of half a second before each new laser melting does not eventually lead to a more complete cooling. With or without delay time, SLM exhibits fast cooling. This is also the reason why the resulting microstructure is much finer than that obtained by LMD. Moreover, due to the cumulative heating and cooling cycles, the microstructure is quite heterogeneous. This is the reason why some heat treatments were applied to homogenize the microstructure.

A first heat treatment was carried out at 900°C for 415 hours under argon. In this case, the initial dendritic structure is decomposed in γ and α_2 grains of approximately 5 μm in size (Figure 4a). A few lamellar colonies can also be detected. The second heat treatment consists of an annealing at 1250°C for 4h under argon followed by air cooling and a further ageing at 900°C for 4h under argon also followed by air cooling, giving rise to a duplex microstructure with lamellar $\gamma+\alpha_2$ colonies as well as γ grains (Figure 4b). A few Nb-rich precipitates are also present at some triple boundaries. Right in the middle of Figure 4b, a large α phase is characterized by some discontinuous coarsening.

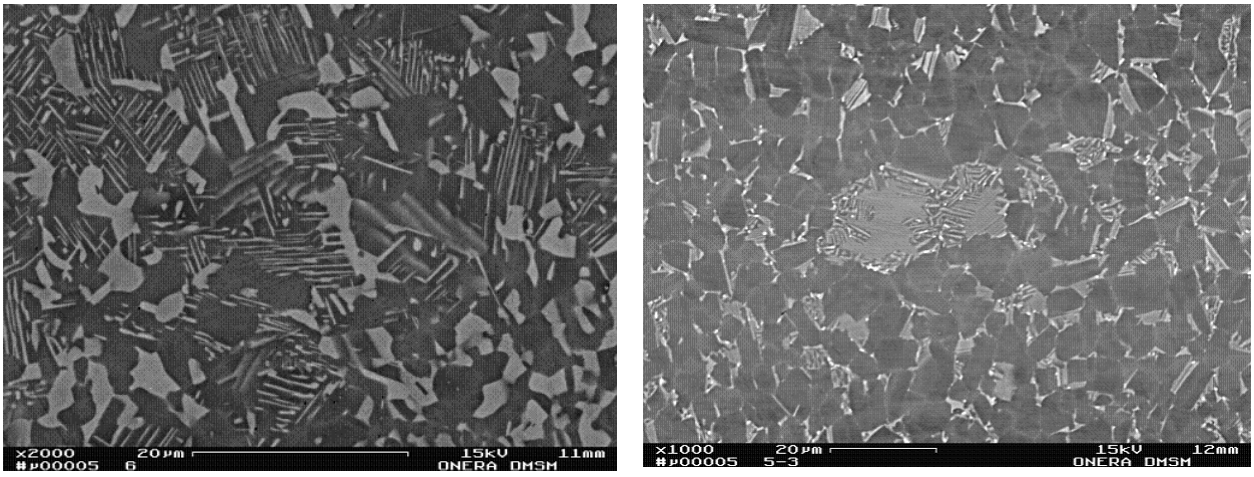

(a) (b)

Figure 4 : SEM micrographs using back-scattered electrons of SLM samples after heat treatments: (a): 415h at 900°C; (b): 4h at 1250°C + 4h at 900°C

The last point under investigation was the possibility to use a recycling powder. First of all, by recycling the powder, the Al content is not changed. Now, regarding the powder morphology, Figure 5a illustrates the fresh powder and Figure 5b the powder which was very close to the melt pool. It appears that powder particles coarser than 50 µm are present in the recycling powder. This is presumably due to liquid droplets extracted from the melt pool and falling in the adjacent powder. A proportion of powder particles exhibits some satellites and some sintering, which means that a complementary sieving of the used powder is necessary before recycling.

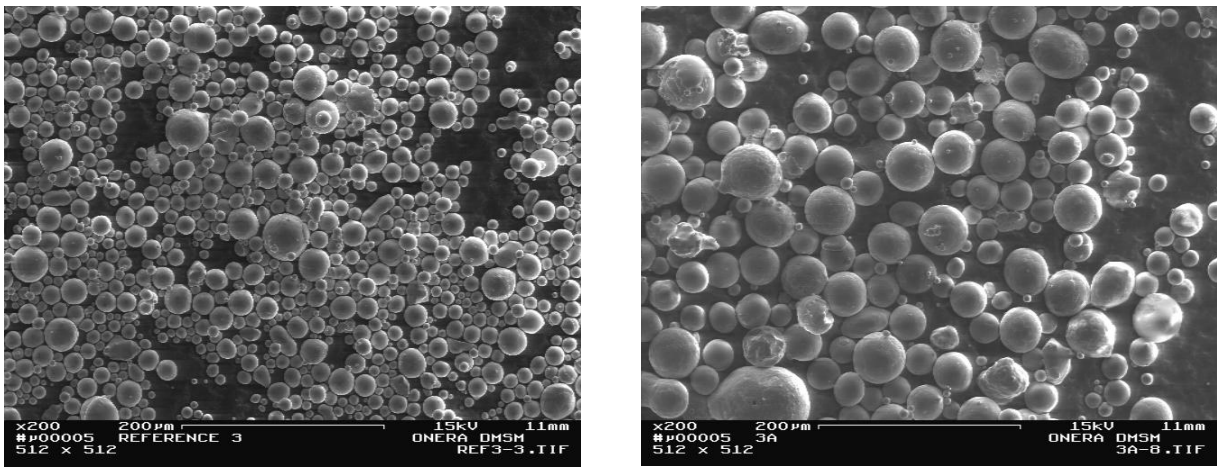

(a) (b)

Figure 5 : SEM micrographs of the TiAl powder; (a): fresh powder; (b) used powder

4. Conclusion

A large number of SLM experiments were conducted under controlled atmosphere by changing the processing parameters to manufacture a series of TiAl beads, XY surface layers and cubes. Whereas LMD process parameters have been identified to eliminate the cracking effect for the TiAl intermetallic alloy, the SLM process induces higher cooling rates that makes difficult to alleviate the cracking effect. By changing the process parameters in the sense that more heat generates lower cooling rate, crack-free samples should be produced. In the present study, the range of process parameters did not allow to completely suppress the cracking effect. Further investigations by changing the process parameters in a larger range and by introducing a preheating source should be able to produce sound bulk TiAl samples.

Conventional post-heat treatment can be successfully used to obtain a more uniform microstructure, which is important to guarantee minimum values for mechanical properties. In that sense, industrial components produced by additive manufacturing appear to be feasible for this intermetallic TiAl material.

Acknowledgements

The authors would like to acknowledge the FRAE (Fondation de Recherche en Aéronautique et Espace) institution for their financial support.

References

1. C.T. Liu, J.H. Schneibel, P.J. Maziasz, J.L. Wright and D.S. Easton: 'Tensile properties and fracture toughness of TiAl alloys with controlled microstructures', *Intermetallics*, 1996, **4**, 429–440.

2. S.F. Clark, 787 Propulsion System. Aero Quarterly; Available from:http://www. boeing.com/commercial/aeromagazine/articles/2012_q3/2/.

3. K. Uenishi and K.F. Kobayashi: 'Processing of Intermetallic Compounds for Structural Applications at High Temperature', *Intermetallics*, 1996, **4**, S95-S101.

4. M. Griffith, C. Atwood, L. Harwell, E. Schlienger, M. Ensz, J.E. Smugereskeym, T. Romero, D. Green and D. Reckaway, Proceedings of the International Congress on Applications of Lasers and Electro-Optics (ICALEO'98), vol. 1, Laser Institute of America, 1998, pp. 1–7.

5. B. Cárcel, A. Serrano, J. Zambrano, V. Amigó and A.C. Cárcel, 'Laser cladding of TiAl intermetallic alloy on Ti6Al4V. Process optimization and properties', *Physics Procedia*, 2014, **56**, 284 – 293.

6. J.H. Moll, E. Whitney, C.F. Yolton and U. Habel, "Laser Forming of Gamma Titanium Aluminide", Gamma Titanium Aluminides 1999, eds. Y-W. Kim, D.M. Dimiduk, M.H. Loretto, H. Clemens and H.H. Rosenberger, The Minerals, Metals & Materials Society, 1999, pp. 255-263.

7. D. Srivastava, D. Hu, I.T.H. Chang and M.H. Loretto, 'The influence of thermal processing route on the microstructure of some TiAl-based alloys', *Intermetallics*, 1999, **7**, 1107-1112.

8. D. Srivastava, I.T.H. Chang and M.H. Loretto, 'The optimisation of processing parameters and characterisation of microstructure of direct laser fabricated TiAl alloy components', *Materials and Design*, 2000, **21**, 425-433.

9. D. Srivastava, I.T.H. Chang and M.H. Loretto, 'The effect of process parameters and heat treatment on the microstructure of direct laser fabricated TiAl alloy samples', *Intermetallics*, 2001, **9**, 1003-1013.

10. X.D. Zhang, C. Brice, D.W. Mahaffey, H. Zhang, K. Schwendner, D.J. Evans and H.L. Fraser, 'Characterization of Laser-Deposited TiAl Alloys', *Scripta materalia*, 2001, **44**, 2419–2424.

11. Y.C. Liu, Z.Q. Guo, T. Wang, D.S. Xu, G.S. Song, G.C. Yang and Y.H. Zhou, 'Directional growth of metastable phase γ in laser-remelted Ti–Al', *Journal of Materials Processing Technology*, 2001, **108**, 394-397.

12. H.P. Qu and H.M. Wang, 'Microstructure and mechanical properties of laser melting deposited γ-TiAl intermetallic alloys', *Materials Science and Engineering A*, 2007, **466**, 187–194.

13. . H.P. Qu, P. Li, S.Q. Zhang, A. Li and H.M. Wang: 'The effects of heat treatment on the microstructure and mechanical property of laser melting deposition γ-TiAl intermetallic alloys', *Materials and Design*, 2010, **31**, 2201–2210.

14. D. Cormier and O. Harrysson: 'Electron beam melting of gamma titanium aluminide'. In: J. Beaman, D. Bourell, editors. Proceedings of 16th solid freeform fabrication symposium, Austin; 2005.

15. D. Cormier, O. Harryson, T. Mahale and H. West, 'Freeform fabrication of titanium aluminide via electron beam melting using prealloyed and blended powders', *Research Letters in Materials Science*, 2007: **4**.

16. L.E. Murr, S.M. Gaytan, A. Ceylan, E. Martinez, J.L. Martinez, D.H. Hernandez, B.I. Machado, D.A. Ramirez, F. Medina, S. Collins and R.B. Wicker, 'Characterization of titanium aluminide alloy components fabricated by additive manufacturing using electron beam melting', *Acta Materialia*, 2010, **58**, 1887–1894.

17. A.R. Rastkar and B. Shokri, 'Surface transformation of Ti–45Al–2Nb–2Mn–1B titanium aluminide by electron beam melting', *Surface & Coatings Technology*, 2010, **204**, 1817–1822

18. S.L. Semiatin, V.G. Ivanchenko, S.V. Akhonin and O.M. Ivasishin, 'Diffusion Models for Evaporation Losses during Electron-Beam Melting of Alpha/Beta-Titanium Alloys', *Metall. Mater. Trans. B*, 2004, **35B**, 235-245.

19. W. Ge, C. Guo and F. Lin, 'Effect of process parameters on microstructure of TiAl alloy produced by electron beam selective melting', *Procedia Engineering*, 2014, **81**, 1192 – 1197.

20. S. Biamino, A. Penna, U. Ackelid, S. Sabbadini, O. Tassa, P. Fino, M. Pavese, P. Gennaro and C. Badini: 'Electron beam melting of Ti-48Al-2Cr-2Nb alloy: Microstructure and mechanical properties investigation', *Intermetallics*, 2011, **19**, 776-781.

21. J. Schwerdtfeger and C. Körner: 'Selective electron beam melting of Ti-48Al-2Cr-2Nb alloy: Microstructure and aluminium loss', *Intermetallics*, 2014, **49**, 29-35.

22. S. Sabbadini, F. Pelissero, S.Biamino, C. Badini, P. Fino, M. Filippini and S. Beretta, 'Third generation gamma TiAl alloys: recent developement at Avio', *International workshop GAT 2013, Toulouse, France.*

23. L. Löber, R. Petters, U. Kühn and J. Eckert, 'Selective Laser Melting of Titaniumaluminides',4th International Workshop on Titanium Aluminides, September 13th - 16th, 2011, Nuremberg, Germany.

24. L. Löber, F. P. Schimansky, U. Kühn, F. Pyczak and J. Eckert, ,Selective laser melting of a beta-solidifying TNM-B1 titaniumaluminide alloy', *Journal of Materials Processing Technology*, 2014, **214**, 1852–1860.

25. M. Thomas, T. Malot and P. Aubry, 'Laser Metal Deposition of the Intermetallic TiAl Alloy', unpublished work, 2016.

Table captions

Table I : Chemical analyses of the initial powder

Figure captions

Figure 1: Optical microscopy of beads manufactured by SLM with different speeds: (a): 10 mm / s; (b): 50 mm / s; (c): 70 mm / s; (d): 160 mm / s

Figure 2: Optical microscopy of XY surface layers using the following parameters: power 50 W, speed 60 mm/s, distance between two laser lines 200 µm

Figure 3 : SEM micrographs using secondary electrons of the surface of SLM samples using the following parameters: power 50 W, speed 50 mm/s, distance between beads 160 µm: (a) : cross-strategy ;(b) : double melting strategy

Figure 4 : SEM micrographs using back-scattered electrons of SLM samples after heat treatments: (a): 415h at 900°C; (b): 4h at 1250°C + 4h at 900°C

Figure 5 : SEM micrographs of the TiAl powder; (a): fresh powder; (b) used powder